UDK 669.15-194
Original scientific article/Izvirni znanstveni članek

ISSN 1580-2949
MTAEC9, 56(6)645(2022)

PROPERTIES OF HIGH-CHROMIUM CAST IRON/LOW-CARBON STEEL BIMETAL FABRICATED BY HOT-ROLLING

LASTNOSTI VROČE VALJANEGA BIMETALA IZDELANEGA IZ KROMOVE LITINE IN NIZKOOGLJIČNEGA JEKLA

Guofeng Yuan[1,*], Xianke Xiao[2], Fei Zhao[1]

[1]School of Mechanical Engineering, Anyang Institute of Technology, Anyang, China
[2]Henan Ancai Hi-Tech Co., Ltd., Anyang, China

Prejem rokopisa – received: 2022-08-05; sprejem za objavo – accepted for publication: 2022-10-10

doi:10.17222/mit.2022.589

A bimetal composite plate including a high-chromium cast iron (HCCI) and low-carbon steel (LCS) cladding was fabricated with hot-rolling bonding in the form of a sandwich structure. In this work, the microstructure and mechanical properties of the bimetal composite were analyzed. Experimental results showed that the brittle HCCI layer achieved good thermoplastic deformation under the action of carbon-steel cladding. After hot rolling, the two metals were well bonded due to mechanical and metallurgical bonding, showing an excellent joint. C atoms diffused uphill the interface. A decarburization area was formed near the LCS side and a fine pearlite diffusion band with a thickness of about 2–3 μm was formed on the bonding interface. The tensile strength of the bimetal composite was 249.5 MPa, and a cleavage fracture appeared on the HCCI side. Interfacial delamination cracks and tunnel cracks of the HCCI were observed in the bimetal composite during a bending test.

Keywords: bimetal, microstructure, hot rolling, mechanical properties

Avtorji so izdelali bimetalno kompozitno ploščo. Sendvič strukturo so izdelali z vročim valjanjem zloženih plošč iz v sredini nameščene močno legirane kromove litine (HCCI) in z obeh strani obdajajočih se plošč iz malogljičnega jekla (LCS). Opisali so analizo mikrostrukture in mehanskih lastnosti izdelane bimetalne kompozitne strukture. Rezultati so pokazali, da se je krhka HCCI plast dobro termoplastično deformirala v objemu dveh plošč iz malogljičnega jekla. Ugotovili so, da je med vročim valjanjem prišlo do dobre medsebojne mehanske in metalurške vezi z nastankom odličnega spoja. Ogljikovi atomi so difundirali navzgor na meji med ploščami. Na strani blizu LCS je prišlo do razogljičenja in na meji je nastala tanka perlitna difuzijska plast debeline približno 2 μm do 3 μm. Izmerjena natezna trdnost bimetalnega kompozita je bila 249,5 MPa. Med porušitvijo je nastal cepilni lom na HCCI strani. Med postopkom upogibnega testiranja bimetalnega kompozita so opazili nastanek mejnih delaminacijskih in prečnih razpok v HCCI.

Ključne besede: bimetal, mikrostruktura, vroče valjanje, mehanske lastnosti

1 INTRODUCTION

High-chromium cast iron (HCCI) with high hardness and excellent wear resistance has been utilized for a long time in cement manufacturing, steel making and mineral processing.[1–4] The HCCI has a higher volume fraction of hard and coarse M_7C_3 Cr-carbides. While these hard Cr-carbides give the HCCI good wear resistance, they also reduce its toughness.[5] In addition, the poor welding performance and plastic deformation ability of the HCCI also limit its application in practical industrial fields.[6]

Bimetal composite materials, which can effectively combine the advantages of two materials, have been used more and more frequently in industry because of their excellent mechanical properties, corrosion resistance and light-ion irradiation resistance, etc.[7–11] Recently, the HCCI and low-carbon steel (LCS) bimetal composites have been fabricated in various ways, such as hot pressing diffusion, surfacing compound, duo-casting, centrifugal casting with hot-rolling and powder metallurgy, etc.[12–24] Sallam et al. prepared the AISI4140 steel and an HCCI bimetal composite through the duo-casting method. The two metals exhibited excellent metallurgical bonding effect through duo-casting.[14] Eroglu et al. found that an increasing bonding temperature and holding time were beneficial to improving the bond strength of the two metals in diffusion bonding.[18] Gao et al. used hot-pressing diffusion bonding to produce a sandwich-structured composite, in which the HCCI was cladded by LCS. They reported that rising the bonding temperature and reducing the strain rate were favorable for improving the bonding strength of the two metals.[19]

Roll-bonding is a common method to prepare a bimetal composite.[25,26] Bimetal composites prepared with this method can achieve good metallurgical bonding between dissimilar metals and improve the microstructure of the component materials effectively. Up to now, there is little research on the solid-solid hot-rolling bonding of HCCI/LCS bimetal composites because of the high crack sensitivity and inherent brittleness of the HCCI. Xie et al. prepared a LCS/HCCI/LCS composite with duo-casting and hot-rolling. Their research revealed that the soft carbon steel cladding exhibited a "lubricating effect" during the common deformation.[21] Similarly, Liu et al.

*Corresponding author's e-mail:
aygxyygf@163.com (Guofeng Yuan)

Table 1: Main chemical compositions (*w*/%) of HCCI and LCS

Material	C	Si	Cr	Mn	P	S	Mo	Ni	Fe
HCCI	2.8	1.1	28	1.0	0.02	0.02	0.5	0.4	balance
LCS	0.12	0.2	0.1	0.5	0.01	0.002	–	–	balance

fabricated a sandwich-structured composite tube with centrifugal casting, and then the blank was hot-rolled at 1170 °C to prepare a bimetal composite plate.[22]

Inspired by the previous studies, an LCS/HCCI/LCS bimetal composite was prepared with solid-solid hot-rolling bonding. In this work, the microstructures of the bonding interface were investigated with a metallographic microscope and scanning electron microscope (SEM). The mechanical properties of the LCS/HCCI/LCS composite plate were evaluated and analyzed with tensile and bending tests.

2 EXPERIMENTAL PART

In this work, the commercial LCS and the as-cast HCCI were used for the ductile part and the wear-resistant part, respectively. The nominal chemical compositions of the two materials are listed in **Table 1**.

Figure 1 displays a schematic representation of the bimetal assembly and the hot-rolling process. Raw sheets were machined to the same size of (5 × 150 × 100) mm. The surfaces of the sheets were polished with a steel brush and cleaned with ethanol before the assembly. The cleared plates were stacked in the LCS/HCCI/LCS pattern, and then the four sides were welded together. Then the slab was vacuumized using a vacuum pump through a reserved air-extraction pipe. The vacuum degree for the slab was less than 1×10^{-3} Pa.

The assembled slab was heated to 1150 °C and held for 30 min. A total of 4 passes of hot rolling were carried out. The accumulated reduction rate was set to be 50 %. The slab was air cooled after the end of the last pass. After hot rolling, a sandwich-structured (LCS/HCCI/LCS) bimetal composite was obtained. The upper LCS layer could be worn out in the process or removed by the machine; then an HCCI/LCS bimetal composite was obtained.

Metallographic specimens were cut from the middle of the plate. The microstructures were observed via an optical microscope (OM) and scanning electron microscope (SEM, Zeiss Sigma-300) with an electron backscatter (EBSD) detector. The EBSD specimen was prepared with electrochemical polishing in a solution of 10 % $HClO_4$ and 90 % C_2H_5OH at 20 V, and the polishing time was 45 s.

To explore the properties of the bimetal composite, tensile tests were performed on a universal testing machine (SHIMASZU, AG-IC100KN) at room temperature with a drawing speed of 1 mm/min. Meanwhile, the digital image correlation (DIC) technique was utilized to measure the localized tensile strains of the thickness direction of the test specimen. The tensile strain was analyzed based on the change in the location of randomly distributed black spots on the surface of the sample.[27,28] The bending specimen was cut into a cuboid with dimensions of (60 × 10 × 7.5) mm and the bending rate was 3 mm/min.

3 RESULTS AND DISCUSSION

3.1 Microstructure

Figure 2a displays a macrograph of a single HCCI plate after hot-rolling at 1150 °C and 30 % total reduction rate. As can be seen, macroscopic cracks perpendicular to the rolling direction can be observed after hot rolling deformation. The single HCCI sheet could not achieve good thermomechanical deformation due to the high crack sensitivity and inherent birttleness.[29] For the composite slab, the bimetal composite material with a sandwich structure can be clearly observed, as shown in **Figures 2b** and **2c**. The brittle HCCI layer in the core achieved good plastic deformation without any cracks. Macroscopically, the two metals achieved good bonding quality without macroscopic cracks or holes at the interface.

The microstructure and EDS results for the bonding interface are displayed in **Figure 3**. **Figures 3a** and **3b** show OM micrographs of the bonding interface. As can be seen, the bonding interface exhibited slight fluctuations, mainly due to the inconsistent deformation of the

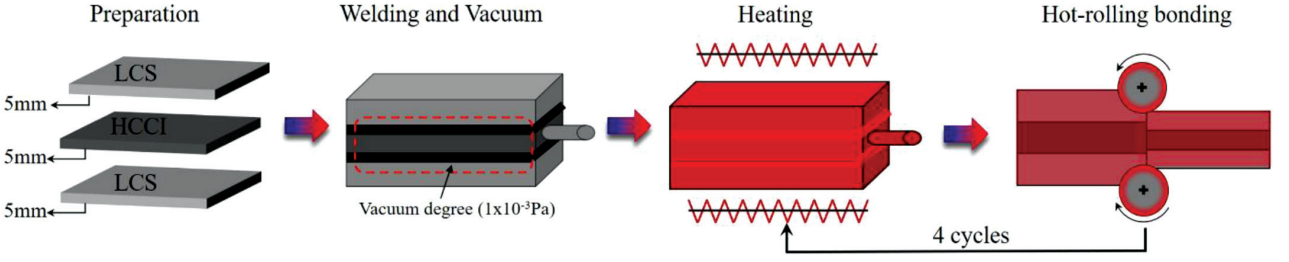

Figure 1: Schematic representation of the bimetal assembly and the hot-rolling process

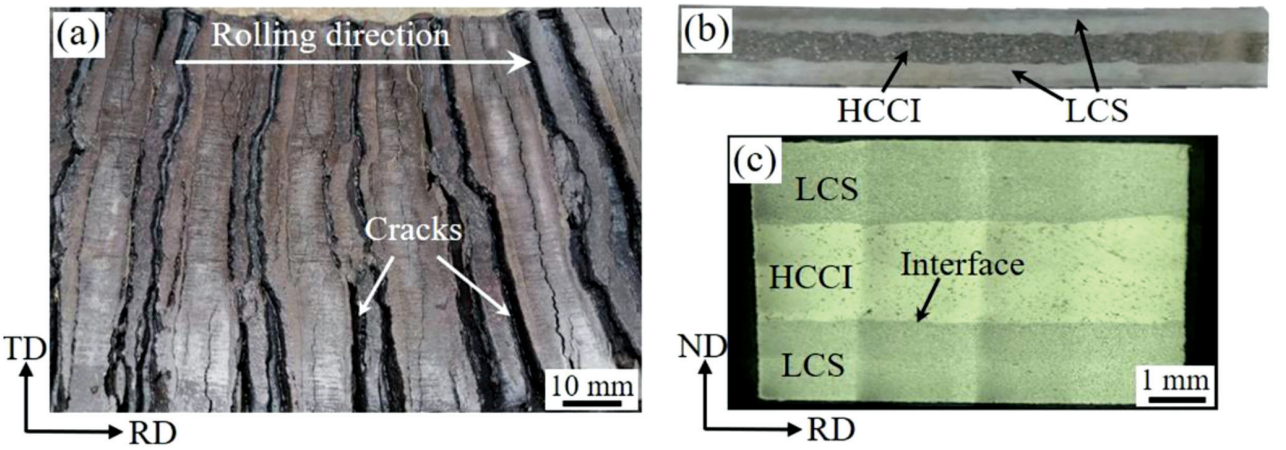

Figure 2: Morphology of the hot-rolled plate: a) single HCCI plate at 1150 °C and 30 % total reduction rate, b) and c) bimetal composite at 1150 °C and 50 % total reduction rate

two metals during hot-rolling deformation.[30] The surfaces of the raw plates to be bonded were mechanically cleaned with a steel brush. The initial mechanical grinding not only increased the surface roughness but also generated a work hardening layer. During hot-rolling bonding, the work hardening layers were broken, and fresh HCCI and LCS metals were exposed. During the subsequent deformation, the HCCI and LCS alloys were put in contact and bonded together.[31]

According to **Figure 3b**, a black narrow diffusion zone with a thickness of about 2–3 μm was detected on the interface and a carbon-poor ferrite zone was observed near the LCS side, indicating that decarburization had occurred. **Figures 3c** and **3d** show SEM micrographs of the interface. It can be seen that the broken oxide particles were dispersed at the interface. As shown in **Figure 3d**, the diffusion zone can be identified as fine pearlite on the high magnification SEM image. Li et al. found a similar interfacial microstructure of the bonding interface between the HCCI and LCS. Their research showed that the chemical potential of C in LCS was higher than that of the HCCI, allowing C atoms to diffuse from the LCS side to the HCCI side.[20]

After hot rolling deformation, the primary carbides of the HCCI fractured into small blocks and were dispersed into the iron matrix, as shown in **Figure 3e.** The fracture refinement of carbides helped improve the overall toughness of the HCCI.[22] **Figures 3g** to **3h** display the corresponding distribution of Cr, Fe and Mn, respectively. According to **Figure 3f**, Fe was mainly distributed in the LCS and the matrix of the HCCI. As shown in **Figure 3g**, Cr was mainly concentrated in M_7C_3 carbides, and the content of Cr detected on the LCS side was minimal.

Figure 4 displays the results of the EBSD analysis of the bonding interface of the RD-ND section. As indicated by the band contrast map of the interface, the two metals were fused together. On the HCCI side, the eutectic carbides and primary carbides were fractured and broken into pieces due to some microcracks, as shown in the red circle in **Figure 4a**. The fracture of Cr-carbides in the HCCI during hot-rolling could effectively reduce the deformation resistance of the matrix

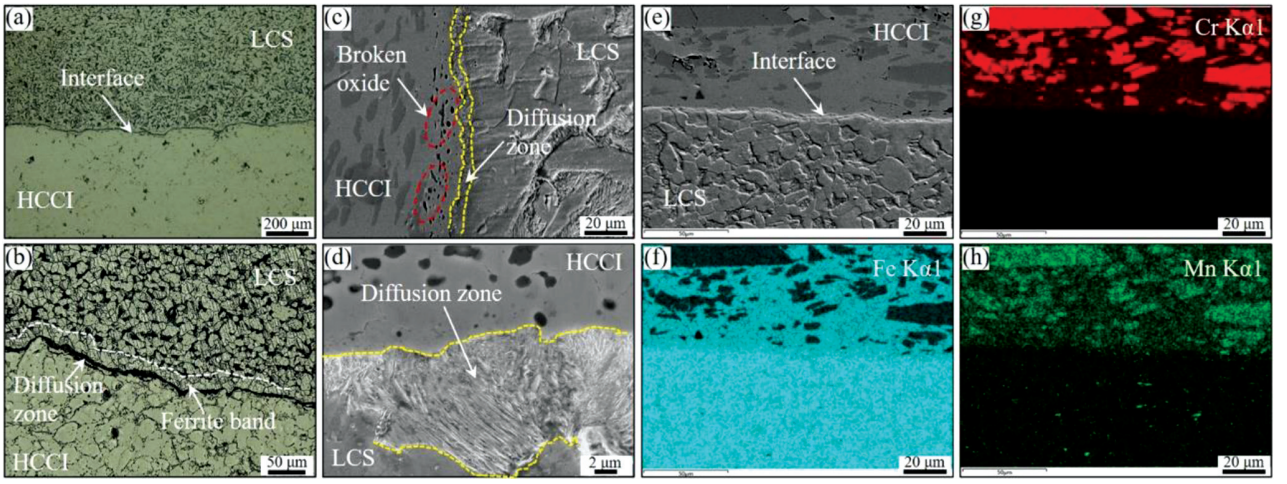

Figure 3: Microstructure of the bimetal composite: a) and b) OM image, c) and d) SEM image, e) to h) results of the EDS analysis

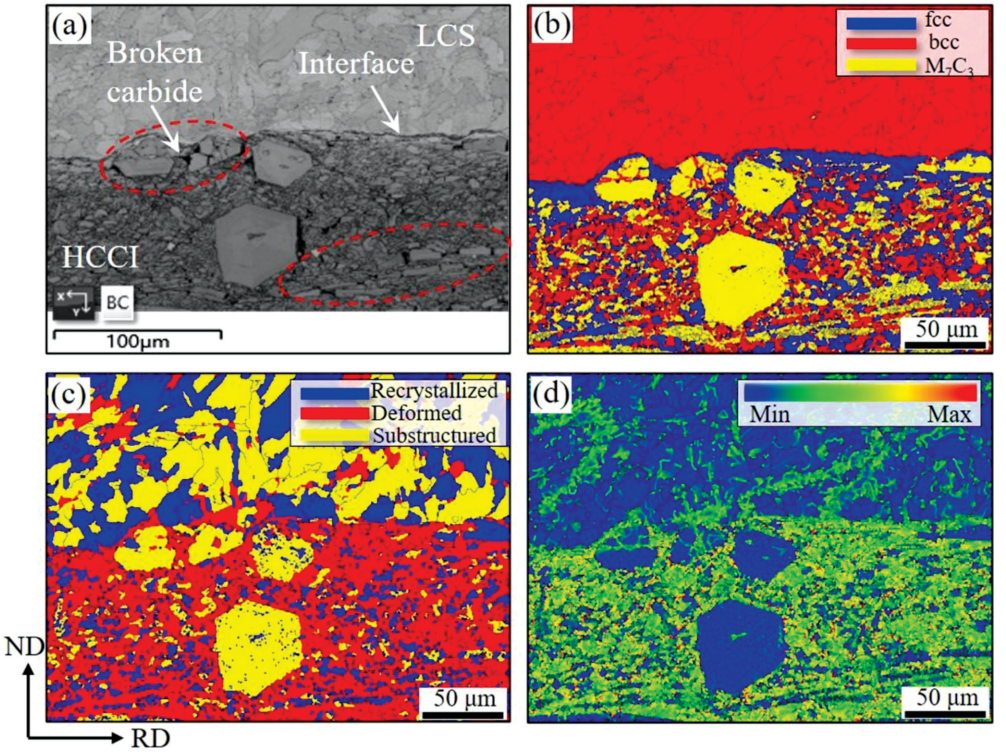

Figure 4: Results of the EBSD analysis: a) band contrast map, b) phase map, c) recrystallization map, d) kernel average misorientation (KAM) map

structure during hot-rolling, which was helpful in the realization of the coordinated deformation between the Cr-carbides and matrix. In the phase map, yellow represents M_7C_3 carbides, red represents bcc and blue represents fcc. The LCS side was composed of ferrite, while the HCCI side included retained austenite, martensite and M_7C_3 carbides. It can be seen from the phase map that the fractured primary carbides and eutectic carbides had a tendency to flow and align along the rolling direction. The recrystallization map of the bonding interface is shown in **Figure 4c** where blue stands for recrystallized grains, red denotes deformed grains, and yellow represents subgrain structures. As can be seen, the recrystallized structure and subgrain structure were the main structures in the LCS layer, while deformed structure was the main structure in the HCCI layer.

Kernel average misorientation (KAM) values can be used as an indicator to describe the local geometrically necessary dislocation (GND) density.[32] According to **Figure 4d**, the KAM has a lower value in the LCS layer. However, the KAM has a higher value in the HCCI layer, especially in the iron matrix, indicating a higher dislocation density in the matrix. Under the same deformation condition, the HCCI layer accumulated higher strain en-

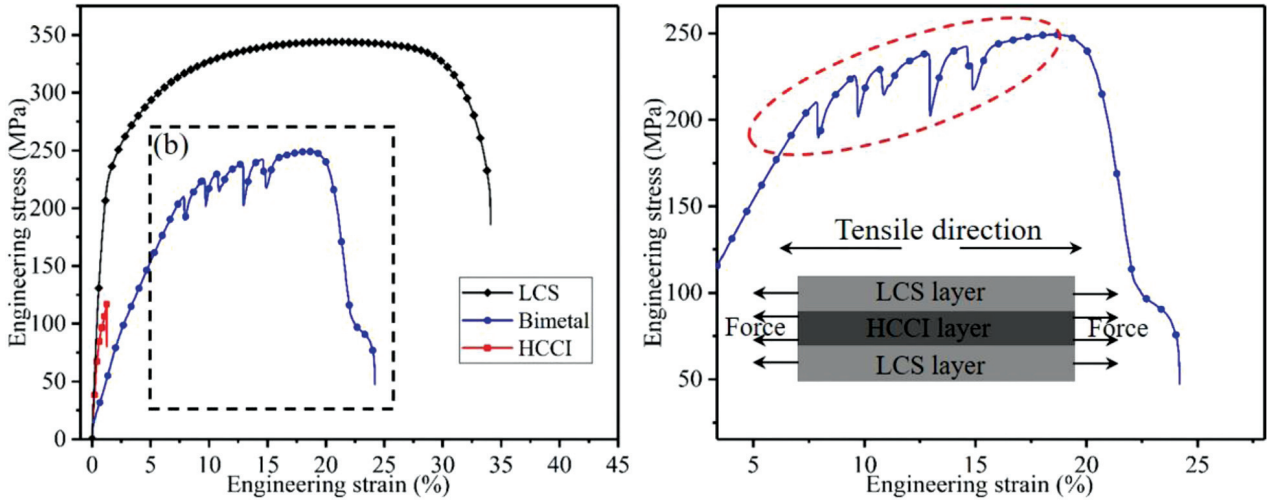

Figure 5: Stress-strain curves of the HCCI, LCS and bimetal composite plate

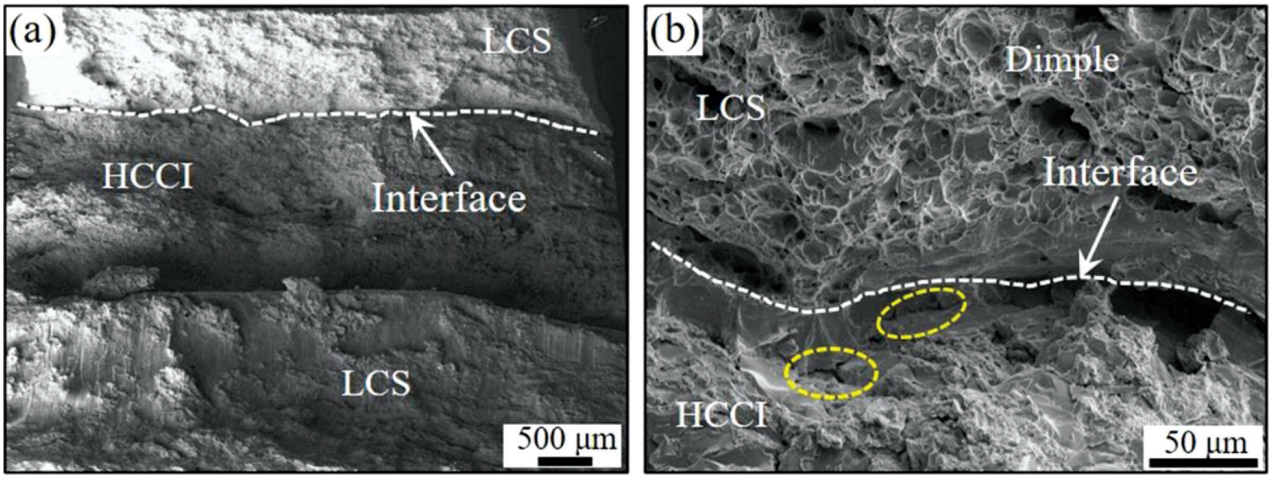

Figure 6: SEM fracture morphology of the bimetal tensile specimen

ergy than that of the LCS layer. The LCS layer consisted of a single ferrite phase (bcc), which had high-stacking fault energy and high dislocation mobility. When the LCS layer deformed, the dislocation density increased continuously. However, some dislocations would be rearranged or eliminated due to the climbing activities or cross-slipping, which reduced the dislocation density of the LCS layer.[33]

3.2 Tensile property

Figure 5 displays tensile stress-strain curves of the as-received HCCI, LCS and the hot rolled bimetal composite. The tensile strength and elongation of the bimetal composite were better than that of the as-cast HCCI and poorer than that of LCS. The average tensile strength of the bimetal reached 249.5 MPa, and the elongation was about 24 %. According to **Figure 5b**, the obvious fluctuations appeared in the stress-strain curve with an increase in the tensile strain. The bimetal composite underwent a "non-catastrophic fracture" stage during tensile deformation.

Figure 6 presents microscopic fracture characteristic of the bimetal composite. As can be seen, no delamination was found at the bonding interface. According to **Figure 6b**, the LCS layer exhibited a ductile fracture, and many dimples were formed near the fracture. However, many cleavage planes and microcracks were detected in the HCCI layer, and its fracture characteristics were typical of a brittle fracture. After the tensile fracture, the two metals were still closely bonded together, reflecting a good metallurgical bonding effect of the two metals.[34]

A digital image correlation (DIC) analysis was carried out to explore the fracture characteristics of the bimetal composite during the tensile process. **Figure 7** shows the strain distribution along the thickness direction of the bimetal composite specimen. It can be seen that no obvious delamination was detected at the bonding interface during the deformation process, indicating

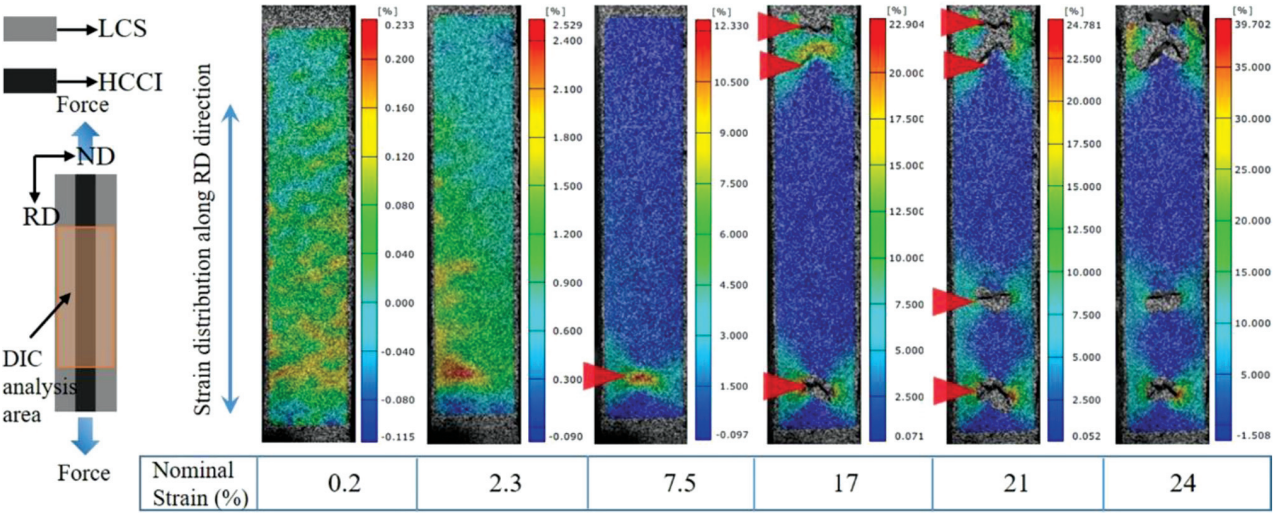

Figure 7: Strain distribution along the thickness direction of the bimetal composite specimen

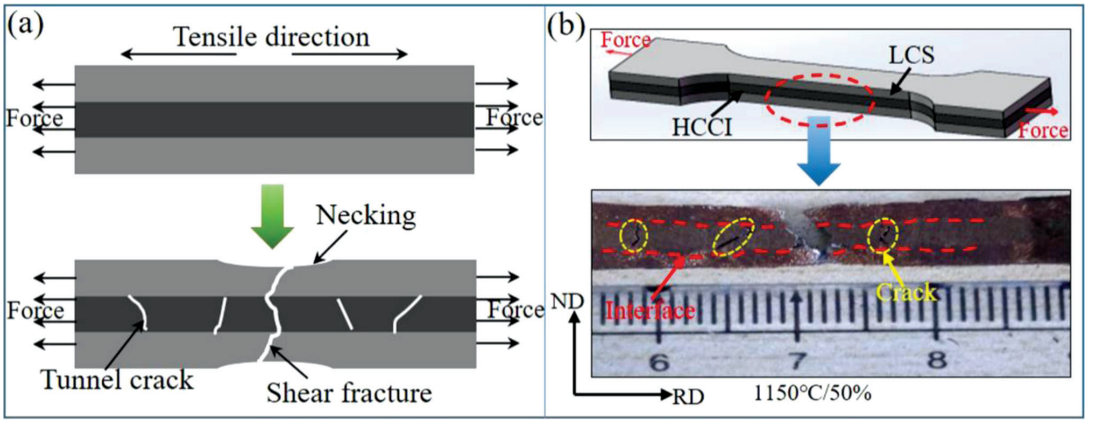

Figure 8: a) Schematic diagram of the fracture mechanism of the bimetal composite, b) macroscopic morphology of the tensile fracture of the specimen

that the two metals obtained good bonding properties after hot rolling. When the nominal strain was 2.3 %, the thickness direction of the tensile specimen showed different degrees of deformation. When the strain increased to 7.5 %, a yellow spot with a larger strain appeared on the surface of the specimen (see the red arrow in **Figure 7**), which may have been the source of the cracks formed due to the cracking of the HCCI layer. It is remarkable that the bimetal composite did not break immediately at the first crack source. Instead, it experienced a step-like fracture process and formed multiple fracture cracks in the HCCI layer, indicating that a series of complicated multiple failures took place. As shown in **Figure 7**, four fracture cracks were formed in the HCCI layer when the strain was 21 %. These complicated multiple failures made the stress fluctuate with the increase in the tensile strain, as shown in **Figure 5**.

Figure 8a shows fracture schematic diagrams of the bimetal composite. During the elastic deformation stage, the HCCI and LCS would deform together under the action of the interfacial bonding force. The strongly bonded interface was sufficient to prevent delamination damage at the interface. The tunnel cracks would firstly occur in the brittle HCCI layer during deformation. The tunnel cracks of the HCCI were perpendicular to the tensile direction and unlikely to extend to the LCS layer, which was important for the toughening of the bimetal. A similar phenomenon was found during the tensile tests of Ti-(TiBw/Ti) composites by Liu et al. Their study reported that the multiple tunneling cracks in TiBw/Ti contributed to the fracture toughness.[35] Compared with the brittle HCCI, the bimetal composite structure could enhance the ability of damage tolerance and energy absorption of the composite.[36] Finally, one of the tunnel cracks expanded into the LCS layer until the composite could

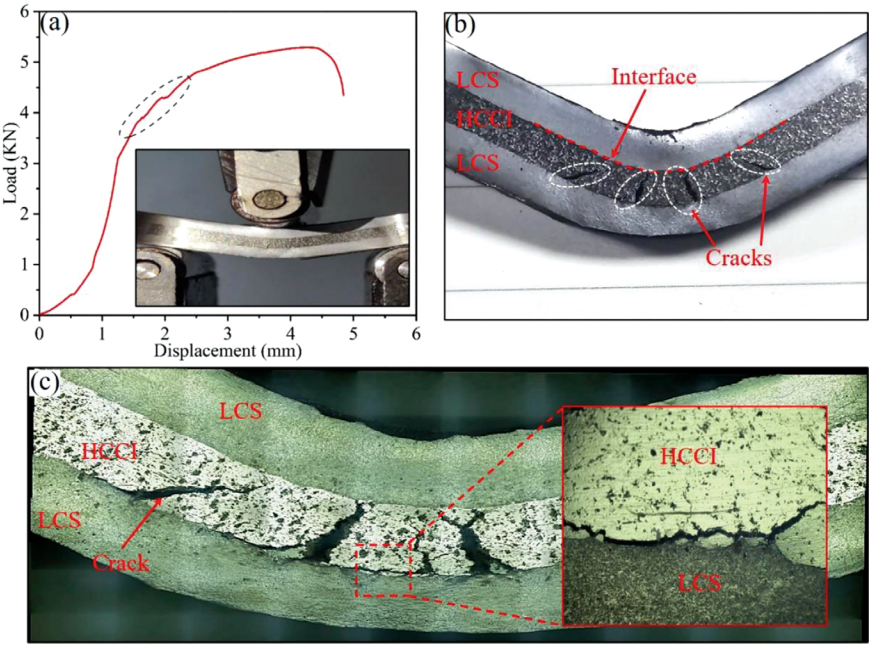

Figure 9: a) Load-displacement curve, b) bending image of the bimetal sample, c) micro-morphology of the fracture

not withstand the increasing stress, resulting in a shear fracture of the LCS, as shown in **Figure 8b**.

3.3 Bending property

The load-displacement curve and bending images of the bimetal sample after a three-point bending test are shown in **Figure 9**. According to **Figure 9a**, when the displacement was about 1.5 mm, the bending curve fluctuated slightly (as shown in the black circle), implying that some cracks were generated during the test process.[37] From **Figure 9b**, it can be seen that there are some fracture cracks in the HCCI layer, corresponding to the fluctuant bending curve from **Figure 9a**.

Figure 9c shows the profile bending fracture characteristics of the bimetal composite. Some interfacial delamination cracks and tunnel cracks were observed in the bimetal composite. The cracks in the HCCI layer stagnated and deflected at the bonding interface, and the LCS layers achieved good plastic deformation. Under the bending condition, cracks would first occur at the maximum stress of the brittle HCCI layer, and the LCS layer revealed plastic deformation. According to the material deformation theory, the tensile stress was below the neutral line (the center line of the HCCI layer). The tensile stress in the bimetal composite can be expressed with the following Equation (1):[38]

$$\sigma_{\text{bimetal}} = E_{\text{bimetal}} \cdot \varepsilon = E_{\text{bimetal}} \frac{x}{\rho} \quad (1)$$

where x represents the distance to the neutral line, and ρ denotes the radius of the curvature. According to Equation (1), the largest tensile stress in the HCCI layer was near the bonding interface below the neutral line. The cracks first formed near the interface when the value of σ_{bimetal} approached the fracture strength of the brittle HCCI. As the degree of bending deformation increased, many tunnel cracks formed and gradually expanded.

4 CONCLUSIONS

1) The brittle HCCI layer exhibited good thermomechanical deformation when hot-rolled at 1150 °C in the form of a sandwich structure. The HCCI and LCS were well bonded after hot rolling bonding at a 50 % cumulative reduction rate.

2) C atoms diffused uphill at the interface, and a carbon-poor ferrite zone was formed near the LCS side. A fine pearlite diffusion zone with a thickness of about 2–3 μm was formed on the bonding interface.

3) Recrystallized structure and subgrain structure were the main structures in the LCS layer, while deformed structure was the main structure in the HCCI layer. The kernel average misorientation presents a higher value for the HCCI layer, especially for the iron matrix, indicating a higher dislocation density of the matrix.

4) The average tensile strength of the bimetal composite reached 249.5 MPa, and the elongation was about 24 %. Interfacial delamination cracks and tunnel cracks of the HCCI were observed in the bimetal composite during the bending test.

Acknowledgments

This work was supported by the National Key Research and Development Program of China (grant number 2018YFA0707304).

5 REFERENCES

[1] X. H. Tang, R. Chung, D. Y. Li, B. Hinckley, K. Dolman, Variations in microstructure of high chromium cast irons and resultant changes in resistance to wear, corrosion and corrosive wear, Wear, 267 (**2009**) 1–4, 116–121, doi:10.1016/j.wear.2008.11.025

[2] S. D. Carpenter, D. Carpenter, J. T. H. Pearce, XRD and electron microscope study of an as-cast 26.6% chromium white iron microstructure, Mater. Chem. Phys., 85 (**2004**) 1, 32–40, doi:10.1016/j.matchemphys.2003.11.037

[3] X. J. Wu, J. D. Xing, H. G. Fu, X. H. Zhi, Effect of titanium on the morphology of primary M_7C_3 carbides in hypereutectic high chromium white iron, Mater. Sci. Eng. A, 457 (**2007**) 1–2, 180–185, doi:10.1016/j.msea.2006.12.006

[4] C. Scandian, C. Boher, J. D. B. de Mello, F. Rézaï-Aria, Effect of molybdenum and chromium contents in sliding wear of high-chromium white cast iron: The relationship between microstructure and wear, Wear, 267 (**2009**) 1–4, 401–408, doi:10.1016/j.wear.2008.12.095

[5] H. S. Ding, S. Q. Liu, H. L. Zhang, J. J. Guo, Improving impact toughness of a high chromium cast iron regarding joint additive of nitrogen and titanium, Mater. Des., 90 (**2016**), 958–968, doi:10.1016/j.matdes.2015.11.055

[6] X. J. Gao, Z. Y. Jiang, D. B. Wei, B. Kosasih, Effect of thermomechanical treatment on sliding wear of high-Cr cast iron with large plastic deformation, Tribol. Int., 92 (**2015**), 117–125, doi:10.1016/j.triboint.2015.06.002

[7] Z. Dhib, N. Guermazi, M. Gaspérini, N. Haddar, Cladding of low-carbon steel to austenitic stainless steel by hot-roll bonding: microstructure and mechanical properties before and after welding, Mater. Sci. Eng. A., 656 (**2016**), 130–141, doi:10.1016/j.msea.2015.12.088

[8] L. Shen, J. Zhou, X. Ma, X. Z. Lu, J. W. Tu, X. Shang, F. Gao, J. S. Zhang, Microstructure and mechanical properties of hot forging die manufactured by bimetal-layer surfacing technology, J. Mater. Process. Technol., 239 (**2017**), 147–159, doi:10.1016/j.jmatprotec.2016.08.020

[9] A. Khadadad, M. Koçak, V. Ventzke, Mechanical and fracture characterization of a bi-material steel plate, Int. J. Press. Vessel. Pip., 79 (**2002**) 3, 181–191, doi:10.1016/S0308-0161(02)00012-1

[10] C. Elanchezhian, B. V. Ramnath, G. Ramakrishnan, K. N. Sripada, M. Muralidharan, V. Kishore, Review on metal matrix composites for marine applications, Mater. Today: Proc., 5 (**2018**) 1, 1211–1218, doi:10.1016/j.matpr.2017.11.203

[11] P. M. Anderson, J. F. Bingert, A. Misra, J. P. Hirth, Rolling textures in nanoscale Cu/Nb multilayers, Acta. Mater., 51 (**2003**) 20, 6059–6075, doi:10.1016/S1359-6454(03)00428-2

[12] H. Oh, S. Lee, J. Jung, S. Ahn, Correlation of microstructure with the wear resistance and fracture toughness of duocast materials composed of high-chromium white cast iron and low-chromium steel, Metall. Mater. Trans. A, 32 (**2001**), 515–524, doi:10.1007/s11661-001-0068-z

[13] C. K. Kim, S. Lee, J. Y. Jung, Effects of heat treatment on wear resistance and fracture toughness of duo-cast materials composed of high-chromium white cast iron and low-chromium steel, Metall. Mater. Trans. A, 37 (**2006**), 633–43, doi:10.1007/s11661-006-0035-9

[14] H. E. M. Sallam, K. Abd EI-Aziz, H. Abd EI-Raouf, E. M. Elabanna, Failure analysis and flexural behavior of high chromium white cast iron and AISI4140 Steel bimetal beams, Mater. Des., 52 (**2013**), 974–980, doi:10.1016/j.matdes.2013.06.045

[15] X. F. Xiao, S. P. Ye, W. X. Yin, Q. Xue, HWCI/carbon steel bimetal liner by liquid–liquid compound lost foam casting, J. Iron. Steel. Res. Int., 19 (**2012**) 10, 13–19, doi:10.1016/S1006-706X(12)60145-9

[16] B. W. Xiong, C .C. Cai, H. Wan, B. P. Lu, Fabrication of high chromium cast iron and medium carbon steel bimetal by liquid-solid casting in electromagnetic induction field, Mater. Des., 32 (**2011**) 5, 2978–2982, doi:10.1016/j.matdes.2011.01.006

[17] B. W. Xiong, C. C. Cai, B. P. Lu, Effect of volume ratio of liquid to solid on the interfacial microstructure and mechanical properties of high chromium cast iron and medium carbon steel bimetal, J. Alloy. Compd., 509 (**2011**), 6700–6704, doi:10.1016/j.jallcom.2011.03.142

[18] M. Eroglu, B. Kurt, Diffusion bonding between high chromium white iron and low carbon steel, Mater. Sci. Tech-Lond., 23 (**2007**), 171–176, doi:10.1179/174328407X154202

[19] X. J. Gao, Z. Y. Jiang, D. B. Wei, S. H. Jiao, D. F. Chen, J. Z. Xu, X. M. Zhang, D. Y. Gong, Effects of temperature and strain rate on microstructure and mechanical properties of high chromium cast iron/low carbon steel bi-metal prepared by hot diffusion-compression bonding, Mater. Des., 63 (**2014**), 650–657, doi:10.1016/j.matdes.2014.06.067

[20] Y. C. Li, M. Y. Gong, K. Wang, P. Li, X. Yang, W. P. Tong, Diffusion behavior and mechanical properties of high chromium cast iron/low carbon steel bimetal, Mater. Sci. Eng. A., 718 (**2018**), 260–266, doi:10.1016/j.msea.2018.01.111

[21] G. L. Xie, J. T. Han, J. Liu, Z. Y. Jiang, Texture, microstructure and microhardness evolution of a hot-rolled high chromium cast iron, Mater. Sci. Eng. A., 527 (**2010**), 6251–6254, doi:10.1016/j.msea.2010.06.036

[22] F. Liu, Y. H. Jiang, H. Xiao, J. Tan, Study on fragmentation and dissolution behavior of carbide in a hot-rolled hypereutectic high chromium cast iron, J. Alloy. Compd., 618 (**2015**), 380–385, doi:10.1016/j.jallcom.2014.07.131

[23] A. Jilleh, N. K. Babu, V. Thota, A. L. Anis, M. K. Harun, M. K. Talari, Microstructural and wear investigation of high chromium white cast iron hardfacing alloys deposited on carbon steel, J. Alloy. Comp., 857 (**2021**), 157472, doi:10.1016/j.jallcom.2020.157472

[24] R. N. Jia, S. L. Liu, Z. C. Luo, J. P. Ning, H. Y. Wang, T. G. Luo, Y. S. Zhu, X. S. Yuan, Z. Wang, Microstructure and Wear Resistance of WC and High Chromium Cast Iron Hardfacing Layers, Coatings, 10 (**2020**) 9, 852, doi:10.3390/coatings10090852

[25] T. Yu, Y. A. Jing, X. L. Yan, W. B. Li, Q. H. Pang, G. Jing, Microstructures and properties of roll-bonded stainless / medium carbon steel clad plates, J. Mater. Process. Tech., 266 (**2019**), 264–273, doi:10.1016/j.jmatprotec.2018.06.007

[26] J. Li, C. R. Liu, Y. H. Song, G. H. Zhao, L. F. Ma, Q. X. Huang, Influence of hot-rolling + heat treatment on microstructure and mechanical properties of NM500/Q345/NM500 composite plate, J. Mater. Sci., 56 (**2021**), 6016–6030, doi:10.1007/s10853-020-05666-4

[27] F. Hild, S. Roux, Digital image correlation: from displacement measurement to identification of elastic properties – a review, Strain, 42 (**2006**), 69–80, doi:10.1111/j.1475-1305.2006.00258.x

[28] M. S. Kim, K. S. Park, D. I. Kim, J. Y. Soh, J. H. Shim, Heterogeneities in the microstructure and mechanical properties of high-Cr martensitic stainless steel produced by repetitive hot roll bonding, Mater. Sci. Eng. A., 801 (**2021**), 140416, doi:10.1016/j.msea.2020.140416

[29] J. Z. Xu, X. J. Gao, Z. Y. Jiang, D. B. Wei, A Comparison of Hot Deformation Behavior of High-Cr White Cast Iron and High-Cr White Cast Iron/Low Carbon Steel Laminate, Steel. Res. Int., 87 (**2016**), 780–788, http://dx.doi.org/10.1002/srin.201500234

[30] P. J. Wang, Z. J. Chen, C. Hu, B. X. Li, J. S. Lin, Q. Liu, Effects of annealing on the interface microstructures and mechanical properties of hot roll bonded Ti6Al4V/AA6061 clad sheets, J. Mater. Res. Technol., 9 (**2020**) 5, 11813–11825. doi:10.1016/j.jmrt.2020.08.070

[31] C. Y. Wang, Y .B. Jiang, J. X. Xie, D. J. Zhou, X. J. Zhang, Interface formation and bonding mechanism of embedded aluminum-steel composite sheet during cold roll bonding, Mater. Sci. Eng. A, 708 (**2017**) 21, 50–59, doi:10.1016/j.msea.2017.09.111

[32] J. S. Li, G. J. Cheng, H. W. Yen, Y. L. Yang, H. Y. Chang, C. Y. Wu, S. H. Wang, J. R. Yang, Microstrain and boundary misorientation evolution for recrystallized super DSS after deformation, Mater. Chem. Phys., 246 (**2020**), 122815, doi:10.1016/j.matchemphys.2020.122815

[33] Y. H. Song, Y. G. Li, G. H. Zhao, H. T. Liu, H. Y. Li, J. Li, E. Q. Liu, Electron Backscatter Diffraction Investigation of Heat Deformation Behavior of 2205 Duplex Stainless Steel, Steel Res. Int., 92 (**2021**) 5, 2000587, doi:10.1002/srin.202000587

[34] B. X. Liu, L. J. Huang, L. Geng, B. Wang, C. Liu, W. C. Zhang, Fabrication and superior ductility of laminated Ti–TiBw/Ti composites by diffusion welding, J. Alloy. Compd., 602 (**2014**), 187–192, doi:10.1016/j.jallcom.2014.02.140

[35] B. X. Liu, L. J. Huang, B. Kaveendran, L. Geng, X. P. Cui, S .L. Wei, F. X. Yin, Tensile and bending behaviors and characteristics of laminated Ti-(TiBw/Ti) composites with different interface status, Compos. Part B: Eng., 108 (**2017**), 377–385 doi:10.1016/j.compositesb.2016.10.001

[36] C. F. Lin, F. C. Jiang, Y. Q. Han, E. H. Wang, Y. Ding, C. H. Guo, Microstructure evolution and fracture behavior of innovative Ti-(SiC_f/Al_3Ti) laminated composites, J. Alloy. Compd., 743 (**2018**), 52–62, doi:10.1016/j.jallcom.2018.01.392

[37] C. M. Cepeda-Jiménez, M. Pozuelo, J. M. García-Infanta, O. A. Ruano, F. Carreñoa, Influence of the alumina thickness at the interfaces on the fracture mechanisms of aluminium multilayer composites, 496 (**2008**) 1–2, 133–142, doi:10.1016/j.msea.2008.05.015

[38] Y. B. Sun, J. Chen, F. M. Ma, K. Ameyama, W. L. Xiao, C. L. Ma, Tensile and flexural properties of multilayered metal/intermetallics composites, Mater. Charact., 102 (**2015**), 167–172, doi:10.1016/j.matchar.2015.02.018